Sensitive All-Optical Channel-Drop Sensor in Photonic Crystals

Yazhao Liu and Huub W. M. Salemink

***Abstract*—We report the results of a study of an optical sensor based on a channel-drop technique with two cascaded cavities in photonic-crystal slabs. Quality factors and intensities of the resonant modes of the sensor were analyzed with three-dimensional simulations. With the introduction of a reflector in the bus-channel and by control of the coupling between the two cavities and the drop-channel, the drop efficiency can be remarkably increased. In addition to the simulation, the two cavity sensor is fabricated and tested for optical response to water and oil infiltration. Both direct visual imaging and quantitative analysis were applied in experiment. A difference of refractive index $\Delta n = 0.12$ between water and oil samples results in a wavelength shift of 18.3 nm, which greatly matches the simulation result of 20 nm and indicates a sensitivity of 153 nm RIU^{-1}. Both resonant peaks for water and oil infiltration have good selectivity in their transmission spectrum. The contrast between the broadband output of the bus-channel and the highly wavelength-selective outputs of the drop-channel opens opportunities for the two cascaded-cavity system as a fundamental building block for a multiplex drop-channel array for all-optical sensing, which can be widely used for bio/chemical detection and environmental monitoring.**

***Index Terms*—Cavity resonators, multiplexing, optical coupling, optical devices, optical sensors, optical waveguide, photonic crystals, photonic integrated circuits.**

I. Introduction

THE application of sensitive micro-scale sensors has become increasingly important in various fields, such as chemical/biological detection and environmental monitoring. Among all kinds of micro-scale sensors [1]–[5], all-optical sensors have attracted many attentions due to their immunity to external electromagnetic field. The principle of operating such passive optical sensors relies on the variation of their optical properties when the refractive index (RI) of the analytic changes [6]–[9]. For the reason of accuracy, investigation of sensors rely on optical resonance are hot research topics [10]–[12]. Optical resonance leads to dips or peaks in the reflection or transmission spectrum. When the refractive indices are modified, wavelength-shifts of the resonance dips or peaks are traceable. With precise calibration, the amplitude of the resonance shift even allows a function of finger-printing.

Manuscript received October 29, 2014; revised May 15, 2015; accepted June 17, 2015. Date of publication June 30, 2015; date of current version August 3, 2015. This work was supported by the program of FOM-IPP IPOG-2: NanoPhotonic Sensors.

Y. Liu is with the Foundation for Fundamental Research on Matter, The Netherlands, and also with the Kavli Institute of Nanoscience, Delft University of Technology, Delft 2628 CJ, The Netherlands (e-mail: liu.delft@gmail.com).

H.W.M. Salemink is with the Institute for Molecules and Materials, Radboud University, Nijmegen 6525 AJ, The Netherlands (e-mail: H.Salemink@science.ru.nl).

Color versions of one or more of the figures in this paper are available online at http://ieeexplore.ieee.org.

Digital Object Identifier 10.1109/JLT.2015.2450995

A good light confinement and a broad free-spectral range are two basic factors for a resonant sensor to fulfill the function of finger-printing. For ring resonators, radii of less than 5 μm are needed to obtain free-spectral ranges over 30 nm [13] in silicon slabs. However, the radiation loss which increases exponentially with the reduction of the radii hindered ring resonators becoming smaller than 3 μm in radii, let alone a real sensing environment usually has high-refractive-index materials surrounded which require larger dimensions to confine light in rings. Photonic crystal sensors, on the other hand, show their advantages to some extent. The number of resonant modes and their free-spectral ranges can be easily adjusted by introducing "defects" in photonic crystals. It has been proved, with fine structural adjustment, a photonic crystal cavity can have a quality factors (Q) as high as 10^6 [14]–[17] in very small dimensions [18], [19], on the order of λ^3. Moreover, sensors used for high-refractive-index sensing with high quality factors and intensities have been developed in our previous works [20], which shown the great possibilities of overcoming the problem of low-index-contrast between photonic crystals and high-refractive-index materials in practical applications.

Another requirement to meet in practical applications is the flexibilities of all-optical sensors in integrating with other elements, especially in lab-on-a-chip devices [21]–[23]. In these components, it is important to read out particular sensing information without disturbing other irrelevant ones. In this paper, to meet the above requirement, we will present our efforts on utilizing the multiplexing technique to modify light in an all-optical channel-drop sensor in photonic crystals. It will be demonstrated in both theory and experiment that drop-efficiency can be greatly increased by introducing one reflector in the bus-channel and controlling the light coupling among cavities and channels.

II. Design

A. Band Structure

The investigated photonic crystal consists of holes etched through a silicon slab. The lattice constant of the photonic crystal is a, and the radii of the holes r are set as $r/a = 0.375$. The thickness h of the silicon slab equals to $h/a = 0.52$ and its RI n_{slab} is set as 3.4. The sensor is embedded in a surrounding material with a RI of $n = 1.5$. Instead of a traditional air-bridge structure, silicon dioxide layer with a thickness of 4a is used as a bottom to support the silicon slab. The confinement of light in the vertical direction is ensured by total internal refection. The dispersion curve of the photonic crystal slab is shown in Fig. 1. Due to the low-index-contrast between silicon and the infilling material, the band gap is rather narrow, ranging from 0.277 to 0.34 in frequency. In order to make the sensor work in

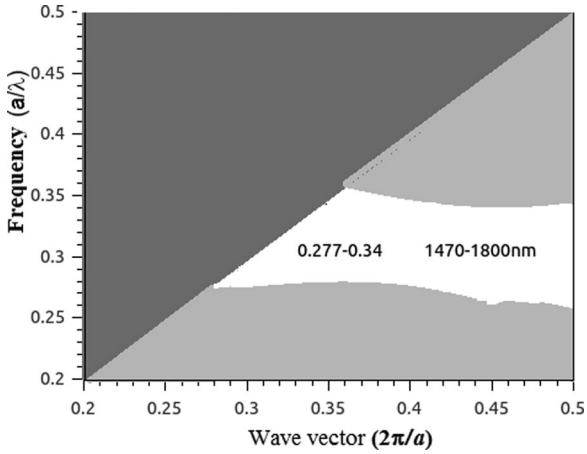

Fig. 1. Band structure of the photonic crystal. A narrow band gap spans from 0.277 to 0.34 in frequency.

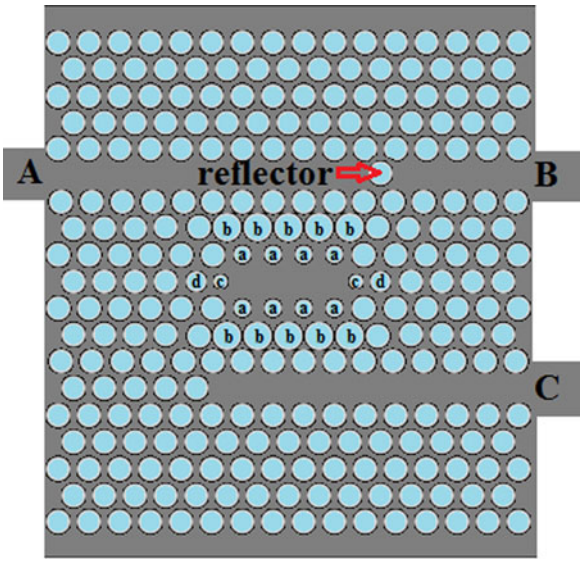

Fig. 2. Photonic crystal sensor with a modified cavity for bus/drop operation. Lattice constant a, radii r. $r_a = 0.72r$ with $\Delta y_a = 0.02a$, $r_b = 1.2r$ with $\Delta y_b = 0.04a$, $r_c = 0.56r$ with $\Delta x_c = 0.21a$, and $r_d = 0.87r$ with $\Delta x_d = 0$.

near-infrared range, we choose the lattice constant $a = 500$ nm. Thus the band gap spans from 1479 to 1800 nm.

B. Single Cavity Sensor

The channel-drop type photonic crystal sensor is schematically shown in Fig. 2. The sensor consist of a fully opened W1 type waveguide (missing a line of holes in the Γ-K direction), a photonic crystal cavity and a half opened W1 waveguide. The upper W1 waveguide serves as a signal bus-channel and the lower one as a receiving drop-channel. Three ports in the sensor are labeled as A, B, C respectively. All ports are connected with stripe waveguides for light input and output. The photonic crystal cavity has the same geometric parameters as described in our previous design [20]. These parameters are selected to optimize the electro-magnetic field overlapping with the analyte in the cavity region. The width of the cavity is modified by locally slightly shifting two neighboring rows of holes away from the center in the Γ-M direction, with shifting distances of $0.02a$ and $0.04a$. The first neighboring row has radius of $r_a = 0.72r$ and the second neighboring row has enlarged radius of $r_b = 1.2r$. The nearest pair of holes to the cavity in the Γ-K direction is shifted $0.21a$ outwardly and reduced to $r_c = 0.56r$ in radius. The next pair also has reduced radius of $r_d = 0.87r$.

The transmission characteristics were simulated with the three-dimensional (3-D) finite-difference time-domain (FDTD) method of MEEP (developed by MIT) using perfectly matched layers with a thickness of $2a$ as absorbing boundaries. A Gaussian optical pulse, covering the whole frequency-range-of-interest, is launched at the input port A. Power monitors were placed at port B and port C to collect the transmitted light. All intensities at the output ports were normalized to the incident light power at the input port A.

Light propagating in the sensor consists of three steps. Incident light from port A transmits along the bus-channel before partially couples to the cavity at the resonant wavelength. A fraction of the resonance photons coupled to the cavity are trapped there for quite a long time, and the remaining fraction couples back to the bus-channel and couples to the drop-channel transmitting towards port C. Apparently, increasing the coupling efficiencies is the key to guide more photons to the drop-channel. The coupling between the input bus-channel and the cavity is optimized first.

As analyzed, a part of the confined light can couple back to the bus-channel and transmit freely to port B: we reduce the waste of this part of light by introducing a reflector in the bus-channel as shown in Fig. 2. The reflector is generated by adding one hole with a radius of $0.375a$. With this reflector, light coupled back to the bus-channel is (at least partially) reflected back towards the input port A. After being reflected at the boundary between the W1 waveguide and the input stripe waveguide, this part of light joins in the incident light and is trapped again by the cavity. The location of the reflector is very important. The reflector should not obstruct light coupling from the input bus-channel to the cavity, nevertheless it must effectively reflect light coupled reversely. Therefore, we position the reflector at the end of the cavity in *x* axis.

Shown in Fig. 3 are the normalized simulated transmission spectra of port C, for the situations with and without the reflector. Note that, for a sensor with the reflector, the resonant peak of the drop-channel is much clearer than that of a sensor without the reflector. The normalized intensity of port C increases from 0.07E–3 to 1.6E–3.

C. Two-Cascaded-Cavity Sensor

The next step is increasing the coupling efficiency between the cavity and the drop-channel. Comparing the photonic crystal cavity with traditional ring resonators, we notice that the largest difference exists in lifetimes of resonances. In micro-ring resonators, light coupling is typically based on phase-matching between orbiting waves in the ring and propagating modes in the waveguide. The orbiting waves propagate along the ring have longer light-paths than the waveguide. The long

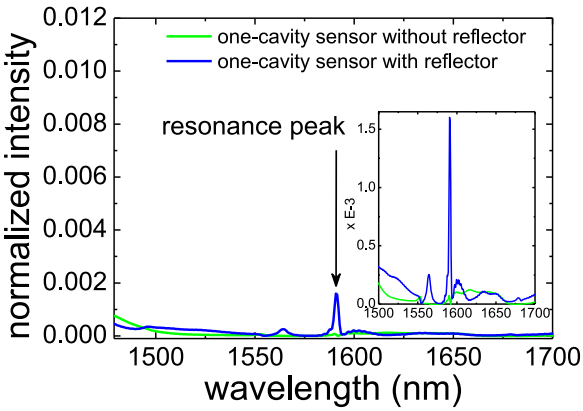

Fig. 3. Calculated transmission spectra of the port C in the one-cavity sensors with and without the reflector. The fill-in material has a RI of $n_{\text{fill}} = 1.5$. The zoom-out spectra keep the same scale as in Fig. 5. Detailed spectra of the sensors are presented in the inset.

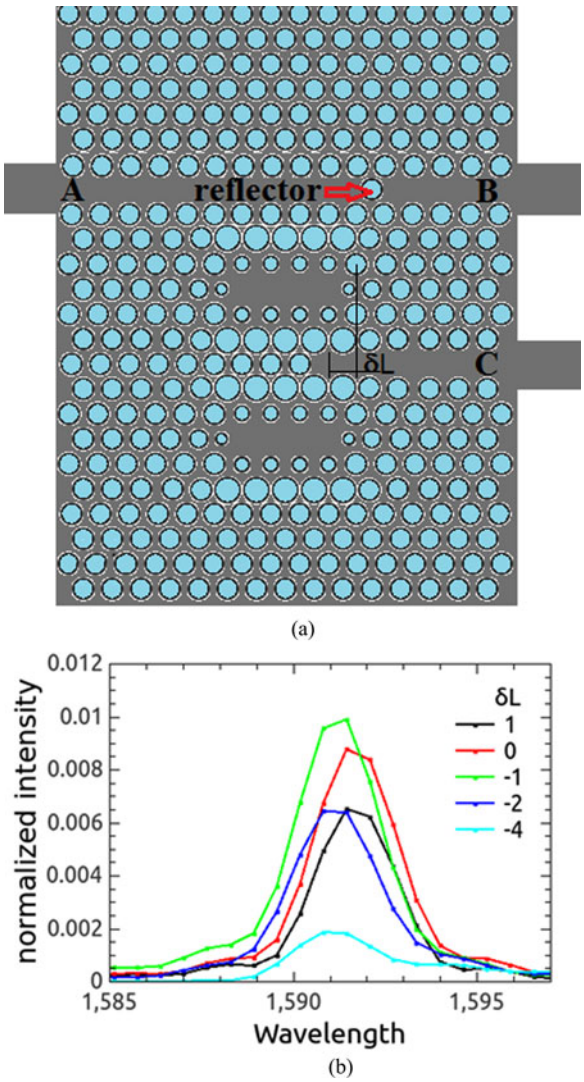

Fig. 4. (a) Optimized photonic crystal sensor with reflector and two-cascaded cavities. Overall dimension of the sensor is $8.7 \times 7.5\ \mu\text{m}^2$. (b) Relationship between the coupling efficiency and the location of the drop-channel. δL is defined as the distance between the inner start-point of the drop-channel and the end of the cavity. Coupling efficiency is reflected in the normalized output intensity of port C.

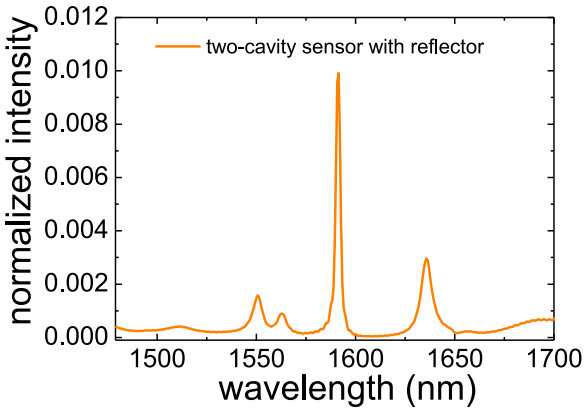

Fig. 5. Calculated transmission spectrum of port C in the optimized sensor. The fill-in material has a RI of $n_{\text{fill}} = 1.5$.

light-paths result in long lifetimes of resonances. Inspired by the same principle, we create a two-cascaded-cavity structure as shown in Fig. 4(a). We add an identical cavity on the mirror side of the first cavity. The two cavities have the same resonant wavelength and can realize a bidirectional coupling between each other. Photons trapped in the first cavity now can reach the third receiver-the second cavity, in addition to coupling to the bus/drop-channels. Resonant light in the second cavity can also couple back to the first cavity and to the drop-channel. Thus, with the reflector and the two cavities, light coupling and recycling are repeated until the whole system reaches a steady state.

It should be noticed that the position of the drop-channel in a two-cascaded-cavity system is similar to the position of the reflector as discussed above. The drop-channel should not block the coupling between the two cavities, meanwhile must effectively receive the in-coupled light. We define the distance between the inner start-point of the drop-channel and the end of the cavity as δL, and mark it in Fig. 4(a). The drop-channel is distant from the two cavities for any positive δL, while in between the two cavities for any negative δL. The influence of δL on the coupling efficiency is described in Fig. 4(b). As can be seen from the black and the red lines in Fig. 4(b), as the drop-channel gradually approach the two cavities from positive δL, the light intensity of the drop-channel increases due to an enhanced coupling from the cavities to the drop-channel. However, the intensity decreases when the drop-channel disturbs the coupling between the two cavities by lying in between. As the overlap between the drop-channel and the two cavities keeps increasing from the green line to the azury line in Fig. 4(b), the intensity of the drop-channel drops sharply. At the complete overlap of $\delta L = -4$, the coupling between the two cavities is blocked by the drop-channel, and the intensity under such a situation is nearly as low as in the single cavity structure. We finally optimize the location of the drop-channel as shown in Fig. 4(a) to get the highest coupling efficiency.

By introducing a reflector in the bus-channel and by placing the second cavity, the output intensity of port C is significantly improved. As presented in Fig. 5, at the identical resonant wavelength, light output in the drop-channel of the two-cavity-sensor is now much higher than the single-cavity design. The output

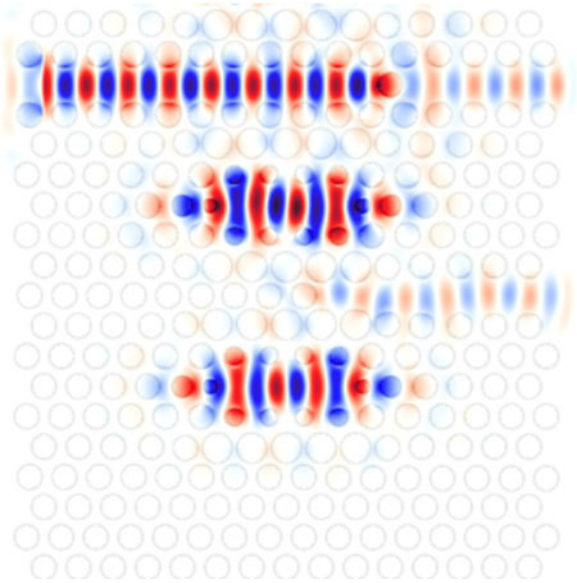

Fig. 6. Simulation of the electric field distribution E_y in the optimized sensor at resonant wavelength. The fill-in material has a RI of $n_{\rm fill} = 1.5$.

intensity of port C now reaches 10E–3, which is ∼140 times higher than the origin value of 0.07E–3. The simulation of the electric field distribution in Fig. 6 confirms the effective light coupling in the optimized sensor.

It should also be noticed that there are three peaks in the transmission spectrum of Fig. 5. The sharpest peak with the highest intensity is the main-resonance of the cavity. The other two peaks are the sub-resonances of the cavity, of which the quality factors and the intensities are much lower than the main resonance as we have discussed in ref [20].

Besides the increased coupling efficiency, another merit of introducing the two-cascaded-cavity structure is to refine the Eigen-resonance of the sensor. Unlike the single-cavity sensor shown in Fig. 2, the two identical cavities in a two-cascade-cavity sensor are distant from the drop-channel. Broadening of the resonant peak caused by lossy-mode-coupling from the bus-channel to the cavity and to the drop-channel is greatly suppressed. The lossy modes are not Eigen-resonance of the cavity. However they can still exist in the cavity for a short time and can be coupled to channels if channels are very close to the cavity. By using the structure in Fig. 4, the mini peaks next to the main resonance around 1600 nm in the insets of Fig. 3 no longer exist in Fig. 5. Similar theory had been demonstrated many years ago in ref. [32], where the distance between a drop-channel and a cavity had crucial influence on the quality of output light.

D. The Principles of Sensing

To illustrate the operating principle of the sensor and to quantitatively estimate its sensitivity, a set of 3-D FDTD simulations has been performed. In these simulations, the holes of the sensor are filled with water and oil of which refractive indices are set to be 1.33 and 1.45, respectively. The calculated output spectra of the drop-channel of the sensor are depicted in Fig. 7(a). Under

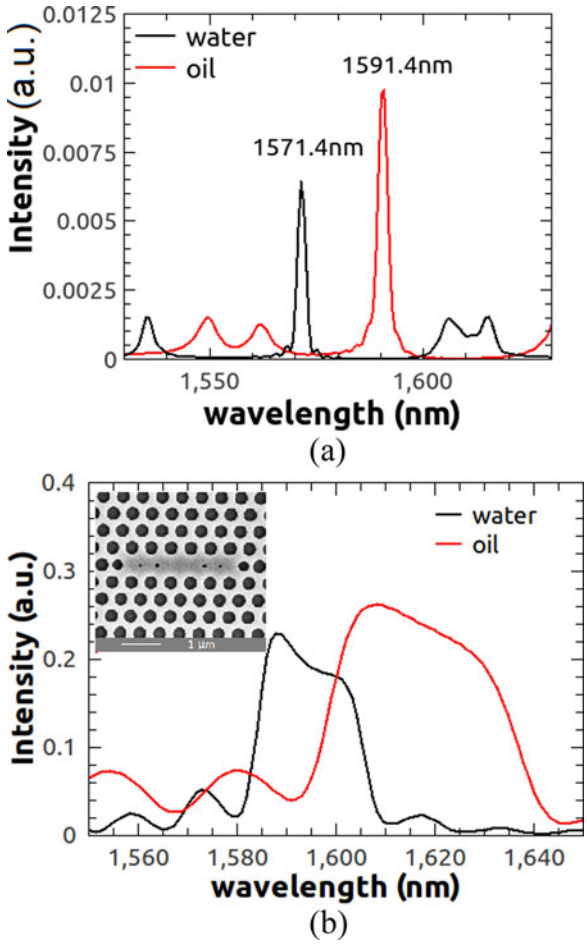

Fig. 7. Calculated transmission spectrum of sensors with water/oil infiltration. (a) A change in the RI of $\Delta n = 0.12$ between water ($n_{\rm water} = 1.33$) and oil ($n_{\rm oil} = 1.45$) results in a spectral shift of 20 nm with the two-cascaded-cavity sensor. (b) Transmission spectrum of the old sensor in ref. [31] with water/oil infiltration. The SEM photo of the old sensor is presented in the inset.

infiltrations, the two peaks in black and red correspond to the calculated resonances, for water and oil respectively. The resonant peaks of water and oil are quite obvious. A change in the RI of $\Delta n = 0.12$ between water and oil results in a spectral shift of approximately 20 nm. As a compare, the sensing ability of our previous design published in ref. [31] for low RI sensing under such liquid infiltrations are also predicted in Fig. 7(b) with a SEM photo of the old sensor as an inset. The resonant peaks in Fig. 7(b) (for both water and oil infiltration in the old sensor) are much broader than those in Fig. 7(a), and there is a large portion of resonant-wavelength-overlap between the two peeks. With such a low quality, it is impossible to sense water and oil precisely.

III. Fabrication

The photonic crystal sensor was realized via fabrication on a silicon-on-insulator (SOI) wafer with a 260 nm-thick silicon membrane and a 2 μm-thick silicon dioxide insulator layer. Fabrication of the device started from cleaning a 2 cm^2 SOI chip with nitric acid to remove any residual organics. ZEP520, a positive electron-beam resist, was spun on top of the SOI chip with

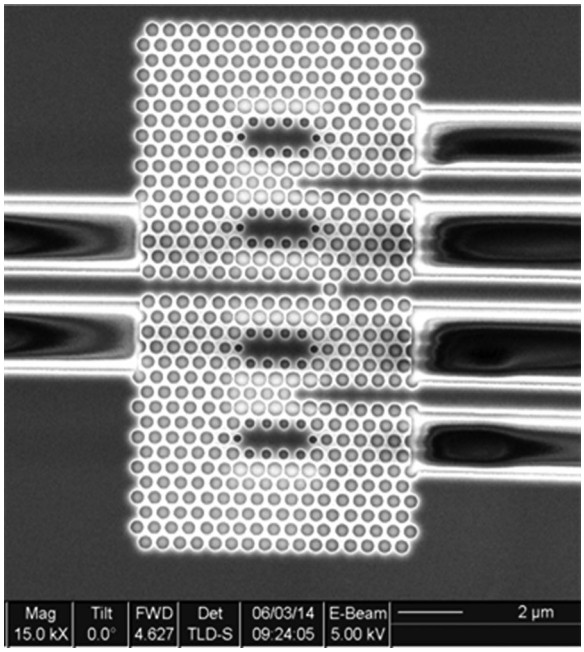

Fig. 8. Scanning electron microscope image of sensor device.

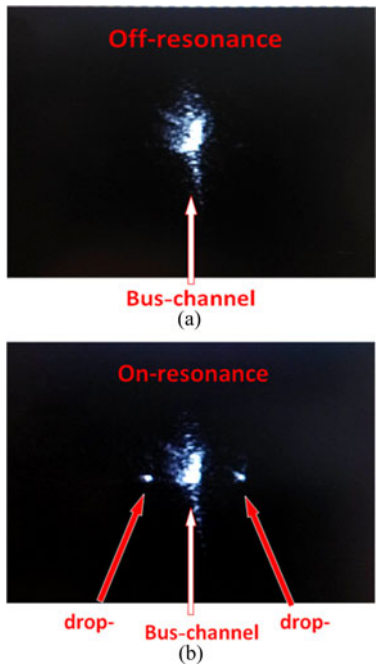

Fig. 9. Images on the screen of the (a) infrared camera off-resonance and (b) on-resonance.

an approximate thickness of 120 nm followed by a pre-baking at 175 °C for 15 min to remove any residual solvent. The photonic crystal was patterned using a Leica EBPG 5000+ e-beam lithography system operating at 100 keV. Exposed areas of the SOI wafer were then etched by the inductively coupled plasma dry etching system of Alcatel AMS100 at the temperature of −120 °C. Following the silicon etching, the remaining ZEP520 was dissolved in PRS3000 solution. Finally IPA was used to remove any surface contaminants and ensured a hydrophilic surface of sensor. The hydrophilicity of the sensor is crucial for our experiment. Hydrophobic or non-hydrophilic surface would cause troubles in liquid infiltration and led to no-resonance as been predicted in our previous work of ref. [20].

For our photonic crystal sensor, the resonant wavelength is set around $\lambda = 1550$ nm. The lattice constant was therefore set to be $a = 500$ nm with hole-radius of $r = 187$ nm. To get a clear visual impression, we made two identical sensors share the same bus-channel as shown in Fig. 8. On each side of the bus-channel, two cascaded cavities and a drop-channel were placed as in the design. Now we have three output channels in total. Coupling into and out of the photonic crystal waveguides are accomplished by traditional tapered strip waveguides. The strip waveguides are 260 nm-thick and taper from 2.5 μm-wide at the chip edge to 866 nm-wide at the photonic crystal waveguide interface, in order to minimize the mode mismatch. The external access to the waveguides is prepared by hand-cleaving.

IV. Experimental Details

A broadband tunable laser of Santec TSL-510 with a wavelengths output ranging from 1440 to 1630 nm was used as our light source. A polarization maintained lensed fiber was used to couple light from the laser to the input strip waveguide. TE polarization was selected before the fiber was mounted onto a three-axis optical stage at an extinction ratio of 100:1. The sample holder also had 3-D flexibilities in fine position adjustment. This setup is identical to our previous reported work. A group of objective lenses focused at the facet of the output strip waveguides, receiving light from the output waveguides. A beam splitter was positioned between the final objective lens and a sensitive photon detector: it tapped part of the light and directed it to an infrared camera. A removable pin hole with a diameter of 200 μm was also placed in front of the beam splitter. Analytes were placed directly atop the sensor via syringes. After each analyte was measured, the liquid drop was blown away from the chip simply by compressed nitrogen gas.

We have scanned the wavelength from 1440 to 1630 nm and observed images of the facet on the screen of the infrared camera. The difference is quite clear in the comparison of the two images in Fig. 9. Since the real sensor-device contains three output ports, one bus-channel and two drop-channels, light can propagate freely in the bus-channel at every wavelength, therefore a clear and large bright spot can always be observed on the screen from the bus transmission. However, the drop-channels have no light propagating through except at the resonant wavelengths. Two more little spots can be observed on the screen only at resonant wavelengths, adjacent to the bus-channel.

The measurement was applied by inserting a pin hole in front of the beam splitter. By moving the position of the pin hole, one particular channel in the sensor can be imaged by the photon detector. We measured the average intensities of the two drop-channels and plot their transmission spectra in Fig. 10. Clearly, in Fig. 10, sharp resonant peaks related to the resonance of cavities. The shifts of the resonant wavelengths depend on the variations of refractive indices. Solid spots in Fig. 10 are original data gotten from experiments, and lines are the Lorentz-fittings

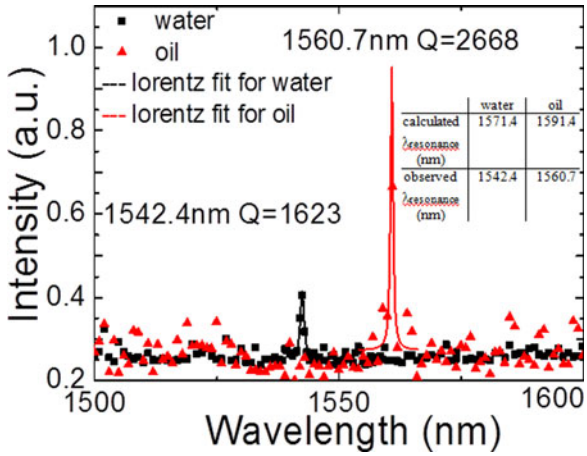

Fig. 10. Experimental transmission spectrum of the optimized sensor. The black and red spots were obtained for water and oil infiltration. A change in RI of $\Delta n = 0.12$ between water ($n_{\mathrm{water}} = 1.33$) and oil ($n_{\mathrm{oil}} = 1.45$) results in a spectral shift of 18.3 nm (from 1542.4 to 1560.7 nm), which is in good agreement with the simulation result of 20 nm in wavelength shift (from 1571.4 to 1591.4 nm).

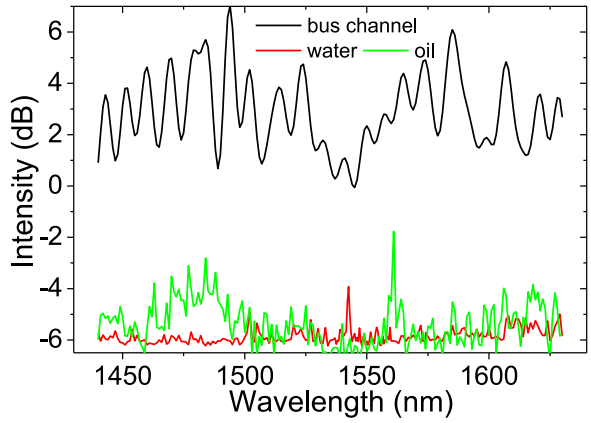

Fig. 11. The contrast between experimental transmission spectra of the bus-channel and the drop-channel under water/oil infiltration.

of those spots. The black spectrum, which corresponds to water-infiltration, shows a Q factor of 1623 at 1542.4 nm. The red spectrum is obtained after the oil sample was filtrated, and its Q factor is 2668 at 1560.7 nm. A ~30 nm blue-shift exists in the wavelength of the entire photonic crystal caused by natural oxidation on the surface and the side walls of the holes [33], as well as by slight fabrication-deviations in the diameter of the holes. We observe very good matches between experimental data and theoretical simulations. For analyte-dependent sensor, the wavelength shift induced by analytes is more meaningful than the absolute resonant wavelength of the photonic crystal cavity. In the presence of increased refractive indices, the wavelength shift is 18.3 nm for water/oil in experiment, while the simulated wavelength shift is 20.0 nm for the same index change. The sensitivity of our sensor is defined as the wavelength shift per RI unit (RIU). A slight index difference of 0.12 results a wavelength shift of 18.3 nm. Therefore, the sensitivity of our sensor is 153 nm RIU^{-1}.

Compare to the drop-channels, the bus-channel maintains a broad band output as illustrated in Fig. 11, except for non-significant decrease in intensity around the resonant wavelengths. This feature allows us to create an inline sensor-system with multi-resonant wavelengths of multi-drop-cavities. As discussed in the chapter of design, the resonant wavelength of the photonic crystal sensor is proportional to the lattice constant, but the quality factors and intensities are dimensionless parameters. A multi-channel sensor system can be formed by simply connecting the bus-channels of many sensor units. Each sensor unit keeps its high quality factor and working wavelength. Different from the filter-designs mentioned in Ref. [24]–[26], the light propagating in the connected bus-channels would not be completely removed after coupling in the drop-channels. However a portion of light can be trapped by a sensor unit at its own resonant wavelength followed by a coupling in a separated drop-channel. The rest of the light can continue its propagation in the bus-channel towards the next sensor unit. The intervals between the resonant wavelengths of the sensor units can be well controlled by carefully choosing the lattice constants.

V. Conclusion

An all-optical photonic crystal-based sensor is demonstrated in this paper. The sensor has a channel-drop configuration with a reflector and an additional photonic crystal cavity. The improved coupling efficiency was confirmed both in theory and in experiment. The sensor keeps a high sensitivity in RI sensing. A minor difference of 0.12 in the RI between water and oil samples results a resonant wavelength shift of 18.3 nm in experiment, which is in excellent agreement with the calculated shift of 20.0 nm. This real wavelength shift results in an index sensitivity of 153 nm RIU^{-1}. We believe that with the small dimension, the prolonged resonance lifetime and the high quality factors, this two-cascaded cavity sensor can be very promising for compacted multi sensor array. Moreover, its compatibility in fabrication with standard semiconductor techniques enables integration with microelectronics, microfluidics [27]–[30] or other photonic devices to fulfill precise sensing in biological, chemical, and medical field.

References

[1] J. Homola, S. Yee, and G. Gauglitz, "Surface plasmon resonance sensors: review," *Sens. Actuators B*, vol. 54, pp. 3–15, 1999.
[2] R. Kunz, "Miniature integrated optical modules for chemical and biochemical sensing," *Sens. Actuators B*, vol. 38, pp. 13–28, 1997.
[3] A. Ymeti, J. Kanger, J. Greve, G. Besselink, P. Lambeck, R. Wijn, and R. Heideman, "Integration of microfluidics with a four-channel integrated optical Young interferometer immunosensor," *Biosens. Bioelectron.*, vol. 20, pp. 1417–1421, 2005.
[4] J. Jensen, P. Hoiby, G. Emiliyanov, O. Bang, L. Pedersen, and A. Bjarklev, "Selective detection of antibodies in microstructured polymer optical fibers," *Opt. Exp.*, vol. 13, pp. 5883–5889, 2005.
[5] L. Rindorf, J. Jensen, M. Dufva, L. Pedersen, P. Hoiby, and O. Bang, "Photonic crystal fiber long-period gratings for biochemical sensing," *Opt. Exp.*, vol. 14, pp. 8224–8231, 2006.
[6] E. Guillermain and P. Fauchet, "Multi-channel biodetection via resonant microcavities coupled to a photonic crystal waveguide," *Proc SPIE*, vol. 7167, art. no. 71670D, pp. 1–11, 2009.
[7] D. Dorfner, T. Zabel, T. Hurlimann, N. Hauke, L. Frandsen, U. Rant, G. Abstreiter, and J. Finley, "Photonic crystal nanostructures for optical

biosensing applications," *Biosens. Bioelectron.*, vol. 24, pp. 3688–3692, 2009.
[8] C. Kang, C. Phare, Y. Vlasov, S. Assefa, and S. Weiss, "Photonic crystal slab sensor with enhanced surface area," *Opt. Exp.*, vol. 18, no. 26, pp. 27930–27937, 2010.
[9] O. Levi, M. Lee, J. Zhang, V. Lousse, S. Brueck, S. Fan, and J. Harris, "Sensitivity analysis of a photonic crystal structure for index-of-refraction sensing," *Proc. SPIE*, vol. 6447, art. no. 64470P, pp. 1–9, 2007.
[10] R. Boyd and J. Heebner, "Sensitive disk resonator photonic biosensor," *Appl. Opt.*, vol. 40, pp. 5742–5747, 2001.
[11] F. Hsiao and C. Lee, "Nanophotonic biosensors using hexagonal nanoring resonators: computational study," *J. Micro/Nanolithogr. MEMS MOEMS*, vol. 10, no. 1, art. no. 013001, pp. 1–8, 2011.
[12] M. Adams, G. DeRose, M. Loncar, and A. Scherer, "Lithographically fabricated optical cavities for refractive index sensing," *J. Vac. Sci. Technol. B*, vol. 23, no. 6, pp. 3168–3173, 2005.
[13] B. E. Little, J. Foresi, G. Steinmeyer, E. R. Thoen, S. T. Chu, H. Haus, E. Ippen, L. C. Kimberling, and W. Greene, "Ultra-compact Si-SiO2 microring resonator optical channel dropping filters," *IEEE Photon. Technol. Lett.*, vol. 10, no. 4, pp. 549–551, Apr. 1998.
[14] Y. Akahane, T. Asano, B. Song, and S. Noda, "High-Q photonic nanocavity in a two-dimensional photonic crystal," *Nature*, vol. 425, pp. 944–947, 2003.
[15] Y. Akahane, T. Asano, B. Song, and S. Noda, "Fine-tuned high-Q photonic-crystal nanocavity," *Opt. Exp.*, vol. 13, no. 4, pp. 1202–1214, 2005.
[16] B. Song, S. Noda, T. Asano, and Y. Akahane, "Ultra-high-Q photonic double-heterostructure nanocavity," *Nature Mater.*, vol. 4, no. 3, pp. 207–210, 2005.
[17] T. Asano, B. Song, and S. Noda, "Analysis of the experimental Q factors ($\sim$ 1 million) of photonic crystal nanocavities," *Opt. Exp.*, vol. 14, no. 5, pp. 1996–2002, 2006.
[18] S. Johnson, S. Fan, P. Villeneuve, and J. Joannopoulos, "Guided modes in photonic crystal slabs," *Phys. Rev. B*, vol. 60, pp. 5751–5758, 1999.
[19] T. Krauss and R. De La Rue, "Photonic crystal in the optical regime-past, present and future," *Prog. Quantum Electron.*, vol. 23, pp. 51–96, 1999.
[20] Y. Liu and H.W.M. Salemink, "All-optical on-chip sensor for high refractive index sensing in photonic crystals," *Europhys. Lett.*, vol. 107, p. 34008, 2014.
[21] N. Mortensen, S. Xiao, and J. Pedersen, "Liquid-infiltrated photonic crystals: Enhanced light-matter interactions for lab-on-a-chip applications," *Microfluid. Nanofluid.*, vol. 4, nos. 1/2, pp. 117–127, 2008.
[22] S. Buswell, V. Wright, J. Buriak, V. Van, and S. Evoy, "Specific detection of proteins using photonic crystal waveguides," *Opt. Exp.*, vol. 16, no. 20, pp. 15949–15957, 2008.
[23] X. Serey, S. Mandal, and D. Erickson, "Comparison of silicon photonic crystal resonator designs for optical trapping of naomaterials," *Nanotechnology*, vol. 21, art. no. 305202, pp. 1–8, 2010.
[24] A. Shinya, S. Mitsugi, E. Kuramochi, and M. Notomi, "Ultra small multiport channel drop filter in two dimensional photonic crystal on silicon-on insulator substrate," *Opt. Exp.*, vol. 14, pp. 12394–12400, 2006.
[25] H. Takano, B.-S. Song, T. Asano, and S. Noda, "Highly efficient multichannel drop filter in a two-dimensional hetero photonic crystal," *Opt. Exp.*, vol. 14, pp. 3491–3496, 2006.
[26] Z. Qiang, W. Zhou, and R. A. Soref, "Optical add-drop filters based on photonic crystal ring resonators," *Opt. Exp.*, vol. 15, pp. 1823–1831, 2007.
[27] S. Mandal and D. Erickson, "Nanoscale optofluidic sensor arrays," *Opt. Exp.*, vol. 16, no. 3, pp. 1623–1631, 2008.
[28] M. Loncar, A. Scherer, and Y. Qiu, "Photonic crystal laser sources for chemical detection," *Appl. Phys. Lett.*, vol. 83, no. 26, pp. 4648–4650, 2003.
[29] M. Adams, M. Loncar, A. Scherer, and Y. Qiu, "Microfluidic integration of porous photonic crystal nanolasers for chemical sensing," *IEEE J. Sel. Areas Commun.*, vol. 23, no. 7, pp. 1348–1354, Jul. 2005.
[30] S. Mandal, R. Akmechet, L. Chen, S. Nugen, A. Baeumner, and D. Erickson, "Nanoscale optofluidic sensor arrays for dengue virus detection," *Proc. SPIE*, vol. 6645, art. no. 66451J, pp. 1–10, 2007.
[31] Y. Liu and H. W. M. Salemink, "Photonic crystal based all-optical on-chip sensor," *Opt. Exp.*, vol. 20, pp. 19912–19920, 2012.
[32] Z. Y. Zhang and M. Qiu, "Coupled-mode analysis of a resonant channel drop filter using waveguides with mirror boundaries," *J. Opt. Soc. Am. B*, vol. 23, pp. 104–113, 2006.
[33] H. Tao, C. Ren, S. Feng, Y. Liu, Z. Li, B. Cheng, D. Zhang, and A. Jin, "Optical improvement of photonic devices fabricated by Ga+ focused ion beam micromachining," *J. Vac. Sci. Technol.*, vol. B-25, no. 5, pp. 1609–1614, 2007.

Yazhao Liu received the Ph.D. degree in experimental nanophotonics from the Institute of Physics, Chinese Academy of Sciences, Beijing, China, in 2009. During 2009–2010, she was a Postdoctoral Research Fellow with the University of Texas at Austin, Austin, TX, USA. During 2011–2014, she was a postdoc with the Foundation for Fundamental Research on Matter, the Netherlands. Since late 2014, she has been a postdoc with the Delft University of Technology, Delft, the Netherlands, supported by Royal Dutch Shell plc. Her current research interests include both theories and applications of nanophotonic structures in extreme conditions.

Huub W. M. Salemink received the Ph.D. degree in experimental solid-state physics from Radboud University, Nijmegen, the Netherlands, in 1973. He is currently holds a personal professorship at Radboud University. He worked with Philips Research on semiconductor lasers and with RIVM on atmospheric lidar. In 1985, he joined IBM Research, Zurich, Switzerland, until 2001. Further he was a Visiting Professor at the Delft University of Technology (TUDelft), Delft, the Netherlands, and received fulltime positions at the Eindhoven University of Technology, Eindhoven, the Netherlands, and at the Department Chairman Kavli Nanoscience, TUDelft in 2004. He has been instrumental in scientific/technical programs on Nanotechnology in the Netherlands.